Chapter 6

Supersonic Plasma Flows due to Magnetoacoustic Shocks

In this chapter, we study an impulsive plasma outflow in the quiet Sun using multiwavelength observations from the Atmospheric Imaging Assembly (AIA) onboard the Solar Dynamics Observatory (SDO) on 2011 March 30. The outflow rises to the upper solar atmosphere with a high terminal speed of 1250 km s^{-1}. Emissions from multiple SDO/AIA channels (log T(K)=4.7 to log T(K)=7.0), peak at the same time indicating its highly impulsive origin. We obtain the line-of-sight differential emission measure maps and find that the outflow is made up of multitemperature plasma. Investigation of SDO/HMI magnetic field data at its footpoint shows that the emerging flux of negative polarity is oscillating at the period of 442 s. The oscillations are also observed in the intensity of 1600 Å almost co-temporally at the base of the outflow with the almost same period (≈416 s). The ~7.0 min periodicity in the magnetic flux and 1600 Å flux is present both prior to and during the onset, and even after the outflows for the duration of ≈1 h. This indicates that the magnetoacoustic waves are generated and present at the

base of the outflow and interact with the localized small-scale current sheet and associated X-point. Magnetoacoustic waves encounter with the discontinuity at the X-point that may further develop into the fast magnetic shocks leading to the formation of the observed shock cusp and triggering of the impulsive plasma outflows. This work is published in "Monthly Notices of the Royal Astronomical Society" Journal.

Y. K. Rao, A. K. Srivastava, J. G. Doyle, and B. N. Dwivedi, *MNRAS, 70, 2449-2456 (2017)*

6.1 Introduction

The quiet-Sun appears highly inhomogenuous in terms of the plasma and magnetic field structuring, which can be characterised by a large number of small-scale dynamic structures having significant effects on the mass and energy flows to the outer solar atmosphere. It has been observed that different kinds of plasma ejections play an important role in the solar atmosphere, transporting mass and energy which varies spatially as well as temporally and have different origins (e.g., Bohlin et al., 1975; Chae et al., 1998b; De Pontieu et al., 2007b; Filippov et al., 2009; Murawski et al., 2011; Nelson et al., 2013; Rouppe van der Voort et al., 2016; Shibata et al., 2007; Tian et al., 2014a; Young et al., 2007, and references cited there). Various types of such small-scale (approximately 3"−10"), and short lived (approximately 2-15 min) plasma ejecta like Ellerman bombs, explosive events, network jets, spicules, surges etc have been observed, which are driven by various plasma processes (Sterling, 2000).

These features are classified on the basis of their different morphological and physical properties. They have important physical implications due to their assumed influence on the coronal heating to million Kelvin temperatures as well as mass leading to the nascent solar wind. The dynamics of the lower solar atmosphere owes its behaviour to such small-scale

energy release driven by various processes like magnetic reconnection (e.g., De Pontieu et al., 2007a; Innes et al., 1997; Peter et al., 2014; Rouppe van der Voort et al., 2016; Shen et al., 2011; Shibata et al., 2007; Yokoyama & Shibata, 1995), magnetohydrodynamic (MHD) wave activity (e.g., Cirtain et al., 2007; De Pontieu et al., 2004, 2007b; Hansteen et al., 2006; Pariat et al., 2010; Rouppe van der Voort et al., 2007; Shibata et al., 2007, and references cited there) and localized temperature enhancement or other factors (e.g., Bewsher et al., 2003; Filippov et al., 2009; Kamio et al., 2010; Madjarska et al., 2009; Murawski et al., 2011; Reid et al., 2017; Shimojo et al., 1996; Teriaca et al., 2001; Tian et al., 2014a, and references cited there). The multi-wavelength observations of highly dynamical small-scale transients help us in understanding the hot plasma embedded in the complex magnetic field. Understanding the driving mechanisms behind such impulsive events is one of the key problems in solar physics research.

These small-scale energetic transients due to strong-magnetic reconnection at the photosphere and different layers of the solar atmosphere have also been reported in ultraviolet (UV) and extreme ultraviolet (EUV) lines (e.g., Filippov et al., 2009; Innes et al., 1997; Nishizuka et al., 2008; Sterling et al., 2012; Yankova & Filipov, 2014, and references cited there). This implies that they drive enormous amount of heat to the transition region and corona locally and may contribute to maintaining the background temperature of the corona to million (~1 MK) degrees of Kelvin (e.g., De Pontieu et al., 2011; Parker, 1988; Porter et al., 1987).

The transportation of the heated coronal mass of temperature between ~0.02 to ~0.1 MK from the lower atmosphere by processes like magnetoconvection contribute significantly to the coronal heating mechanisms (e.g., Alexander et al., 2001; McIntosh et al., 2007; Simon et al., 1989, and references cited there).

On the other hand, it is also well established that global acoustic modes with different frequencies prevail all over the surface of the Sun. These acoustic oscillations show their

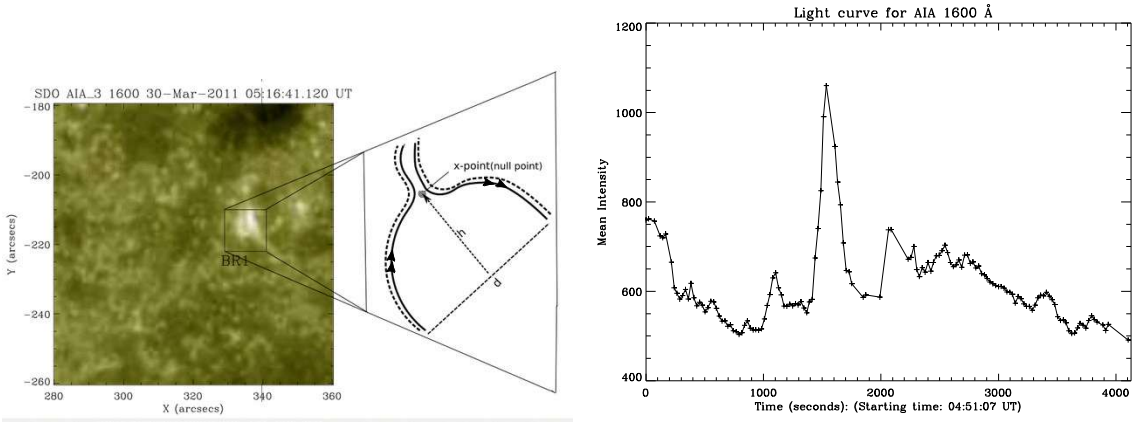

Figure 6.1: (a) Identification of brightening and energy release site at the top of the photosphere as observed by SDO/AIA 1600 Å . A small-scale curent sheet and X-point is evident at the base of the outflow as shown also in the schematic. (b) Light curve derived from the selected box showing the variation of intensity with time.

effects by leakage of their energy from the photosphere along the strongly magnetized flux tubes and can launch the chromospheric spicules (e.g., De Pontieu et al., 2004, 2007a; Rouppe van der Voort et al., 2007). Such acoustic drivers (2.5 - 7.5 min) may propagate from the photosphere upwards in magnetized regions in the form of magnetoacoustic waves (e.g., Bogdan et al., 2003; Fedun et al., 2009; Hansteen et al., 2006). The perturbations causing such magnetoacoustic waves or shocks may also be able to launch oscillatory reconnection, and associated wave activities in localized magnetic field domains (e.g., flux tubes and current sheets), which may also launch plasma jets and flows (Bulanov & Syrovatskii, 1980; Craig & McClymont, 1991; Heggland et al., 2009; McLaughlin et al., 2009, 2011). However, the direct observational signature of such events are very rare.

In the investigation of such physical processes, we study extremely impulsive plasma outflows in the quiet-Sun region using observations from the Atmospheric Imaging Assembly (AIA; Lemen et al. 2012) and Helioseismic Magnetic Imager (HMI; Scherrer et al. 2012) onboard Solar Dynamics Observatory (SDO) on 2011 March 30. We also study the linkage between the observed outflows and the underlying photospheric magnetic fields as well as associated physical processes. In this chapter, we analyse the small-scale energy

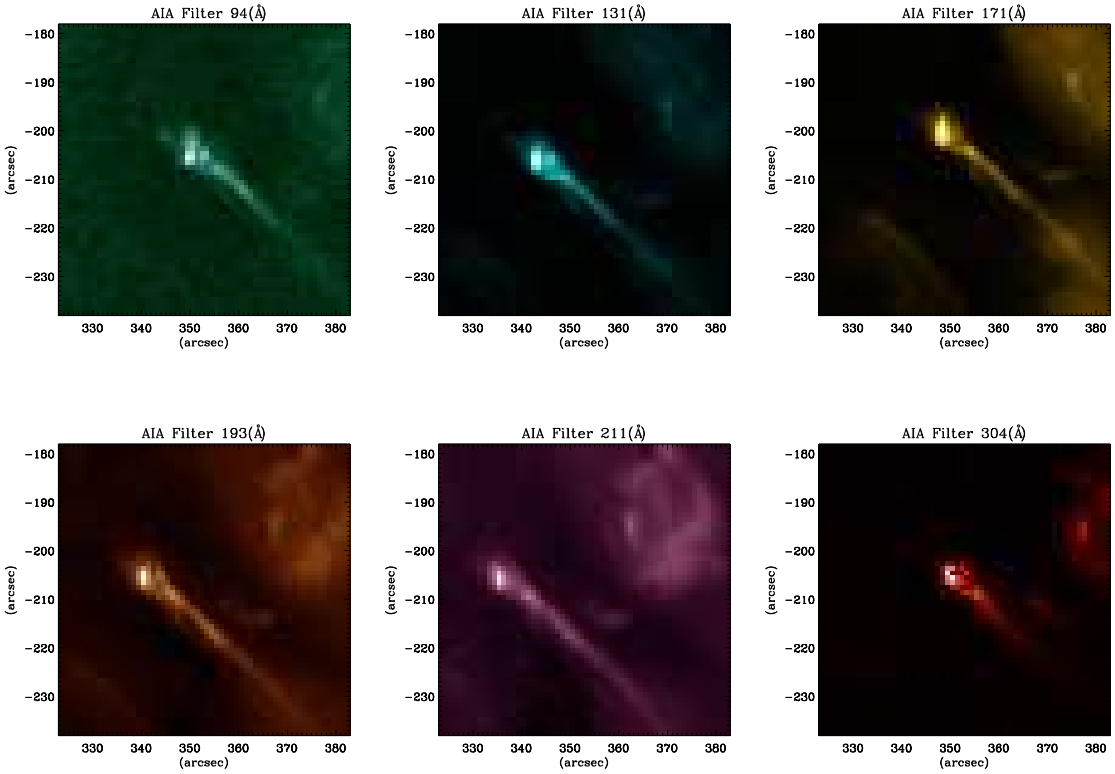

Figure 6.2: The emissions from the impulsive energy release site observed in different filters of AIA at the peak of the plasma outflow at 05:18 UT. All the bands of AIA show a similar morphological behaviour.

transient and associated plasma dynamics. This highly impulsive event is short lived but can be observed from the photosphere propagating up to the upper atmosphere where it fades out and submits all its energy and mass. Sect. 6.2 describes the observational data and its analysis. In Sect. 6.3, we discuss the observational results and driving mechanism of the observed impulsive plasma outflows. In the last section of this chapter, discussion and conclusions are outlined on the basis of the implications of our scientific results.

6.2 Observational Data and Its Analysis

The Atmospheric Assembly Imager (AIA) is a multi-channel full disk imager (Lemen et al., 2012) with spatial resolution of 1.5" with a pixel size of 0.6" and a cadence of 12 s. These data were taken during the period of 04:51:01 UT to 05:59:55 UT on 30th March 2011 observing from near the photosphere to the upper chromosphere and coronal region. For our analysis, we choose a particular area of $\approx$ 250" by 250" FOV ranging from $\sim$ 200" to 450" in the x-direction and -150" to ~ -400" in the y-direction at the southern region of the sunspot (NOAA AR 11759). This AIA region of interest contains different small-scale brightenings over the chosen period of time (04:51:01 UT $-$ 05:59:55 UT). In these small-scale brightenings, we chose the one showing the impulsive rise of the flux in AIA UV 1600 Å continuum (Fig. 6.1).

The HMI has a cadence of 45 s (Scherrer et al., 2012). We have used full-disk LOS magnetogram data having 4096×4096 pixel size. Data from SDO/AIA are studied to conduct a multi wavelength analysis of the impulsive high-speed outflows associated with the brightening as shown in Fig. 6.1. Each SDO/AIA image is cropped to follow the same FOV containing plasma outflows (see Fig. 6.2). To infer the topology of the underlying magnetic field, a two-hour period (between 04:00 UT and 05:59 UT) of data from HMI was also analysed. The HMI data was rotated and aligned with the AIA data to have the same plate scale since these two instruments have different resolutions.

6.3 Observational Results

6.3.1 Properties of localized energy release at the photosphere

The left panel of Fig. 6.1 shows an enlarged view of an image taken in the 1600 Å passband of AIA. The box containing the brightening has also been zoomed to show the configuration of the magnetic field associated with this brightening and the impulsive energy release. The base of the outflow is evident like a small-scale cusp like structure containing the current sheet and a X-point (see the schematic in Fig. 6.1). We consider the complete evolution of this brightening and impulsive energy release. The light curve obtained from this brightening is shown in right panel of Fig. 6.1 where the starting time is 04:50 UT. Light curve for 1600 Å wavelength has been derived from the square box centred at (328", 213") with the size of each side 12. The brightening stays relatively quiet and shows an impulsive peak at 05:18 UT. The intensity variation increases rapidly during the impulsive energy release, which is evidence of an energy release at its base to drive its plasma to the upper atmosphere.

Using the observations taken in other bands of AIA, we find a similar morphological behaviour (see Fig. 6.2). The brightening and associated outflow is most prominently visible in 1600 Å, 171 Å & 211 Å and can also be observed in 131 Å, 304 Å, 335 Å. Fig. 6.2 shows near simultaneous observations taken using EUV bandpasses of AIA. Fig. 6.3 shows the light curves for all the different filters.

We take the area containing just the single brightening of 60" by 60" in our investigation, which is associated with the base of the observed plasma outflow (Fig. 6.1 and 6.2). The impulsive compact brightening has a size of ≈ 8" and takes ∼8 min for its full evolution and fading out, while, the outflow observed in the quiet-Sun rose above it very rapidly (Fig. 6.4, right panel). This lifetime is the full duration of the streaming of plasma in

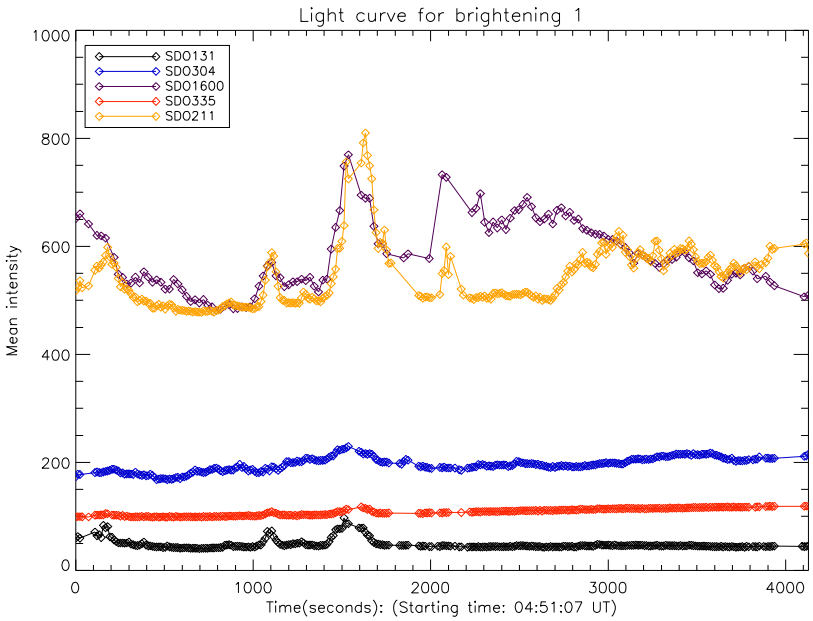

Figure 6.3: The light curves of co-temporal emissions from the impulsive energy release site at different wavelength filters of AIA. Different colors represent different filters as mentioned.

the outflow as visible in various AIA filters. The kinematics of the fast moving plasma outflow is discussed in sub-section 6.2. The similar brightening feature has been observed in all other EUV (94 Å, 131 Å, 171 Å, 193 Å, 211 Å, 304 Å, 335 Å) filters indicating the multi-temperature plasma outflowing impulsively to the upper atmsophere. The impulsive multi-temperature plasma outflows are considered different than typical EUV jets (e.g., Culhane et al., 2007a; Kamio et al., 2010; Nishizuka et al., 2008) due to the fact that there is no evidence of time-lag between the emissions from various AIA filters, and no spatio-temporal signature of the separate evolution of cool and hot plasma components.

The outflows differ from the very characteristic behaviour of other dynamic phenomena such as EUV jets or surges (Schmahl, 1981) and X-ray jets (Shibata et al., 1992). Surges reach upto the heights of 20,000 km to 200,000 km (Sterling, 2000). Shibata et al. (1992) has also suggested the different driving mechanism for X-ray jets and surges. The heating due to the magnetic reconnection results in X-ray jets while surges result from the dynamic

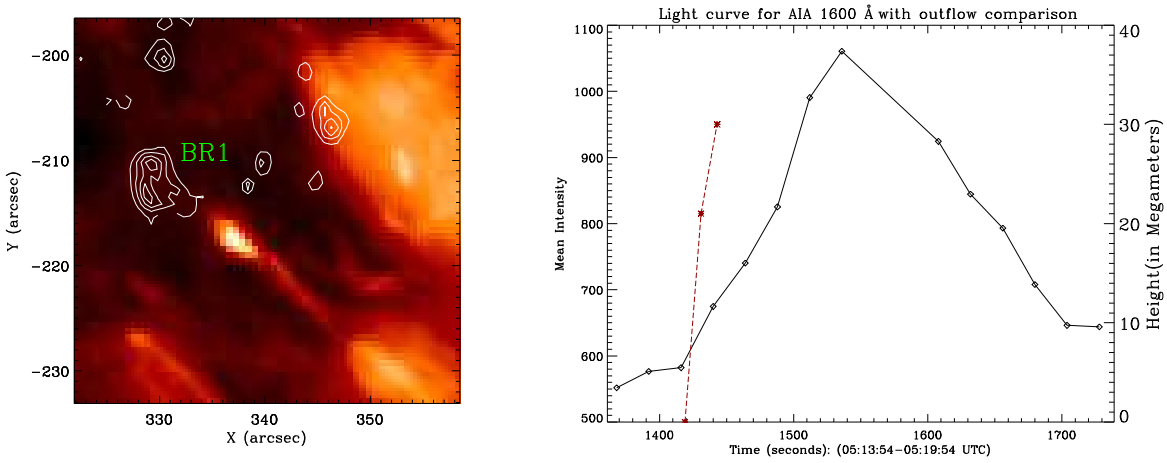

Figure 6.4: Left panel: The plasma outflow associated with the impulsive energy release site. The contours of the 1600 Å wavelength are overlaid on the 193 Å wavelength at 05:18 UT. Right panel: The kinematics of the outflows co-temporal with the initial enhancement of the energy release. The intensity curve is overplotted by the height-time plot which has been obtained by tracing the tip of the outflow starting from the X-point of the small-scale current sheet as shown in the schematic illustration of the Fig. 6.1
.

whip-like motion, and due to the launch of a thermal pulse from the chromosphere (Kayshap et al., 2013). These mechanisms have been confirmed by observations (Canfield et al., 1996). Different kinds of chromospheric jets such as EUV jets and X-ray jets are caused by the magnetic reconnection or deposition of the energy in the higher chromosphere (Sterling, 2000). All these events have lifetimes of 100 – 2000 s, significantly longer than the present feature.

6.3.2 Kinematics of plasma outflows due to impulsive energy release

It is shown in the enlarged field-of-view (FOV) of the small-scale brightening region (Fig. 6.1) that a small current-sheet like cusp shaped structure is formed with a narrow neck at the top. The projected height of the neck from the footpoints of the two halves of this small-scale current sheet is around 5.0 Mm. The reconnection X-point, therefore, lies

in the inner corona, though in a very confined magnetic domain. This morphology can be considered as a miniature version of a typical flare generating region, where reconnection in the corona starts a flare energy release near an X-point (e.g., Benz, 2008). In the typical flaring region, the outside response above the X-point could be a plasmoid ejection. However, in the present case, at small spatio-temporal scales, the reconnection process and associated energy release (Figs. 6.1-6.2) generate a multi-temperature, highly impulsive plasma outflow. The possible trigger of reconnection in this miniature version of X-point typical current sheet is discussed in subsection 6.3. The left panel of Fig. 6.4 displays the AIA 193 Å image showing the outflow overlaid by the 1600 Å continuum contours. The right panel of Fig. 6.4 shows the intensity curve during the outflow overplotted by a height-time plot for the plasma outflow measured using observations recorded in the 193 Å channel. The dashed line represents height-time plot which has been obtained by tracing the tip of the outflow starting from the X-point of the small-scale current sheet. This clearly demonstrates that the outflow suddenly rises to 30 Mm in ≈24 seconds. This provides us with the apparent velocity of the outflow to be ≈1250 km s^{-1}. Although the streaming of the plasma through this ejected outflow channel last about 8.0 min into the corona after its rapid elongation from the origin point. This unique plasma outflow is very rapid and its terminal velocity seems to be equal to almost the local Alfvén velocity in the inner corona.

6.3.3 DEM from energy release site and its multi-thermal nature

In order to understand the thermal structure of the plasma outflow, we derive differential emission measure (DEM) maps at different temperatures from the six AIA channels (94 Å, 131 Å, 171 Å, 193 Å, 211 Å, 304 Å) sensitive to a range of coronal temperatures. We have used an automated method (Hannah & Kontar, 2012) to carry out DEM analysis. We have

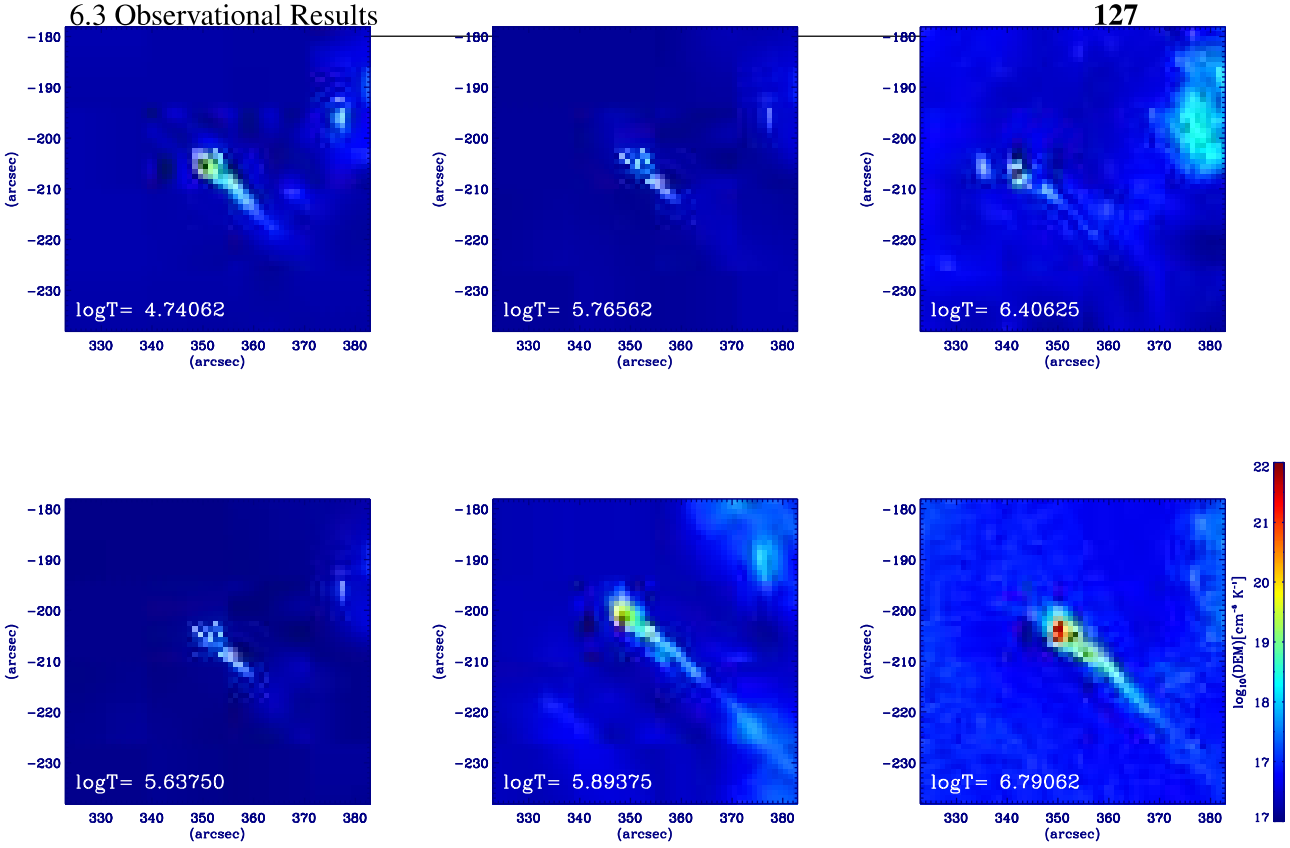

Figure 6.5: Differential Emission Measure (DEM) maps of the outflow at different temperatures of the outflow observed on 30th March 2011

used the selected area of SDO/AIA in all the six channels as mentioned above at the time of maximum rise of the outflow around 05:18 UT on 30th March 2011.

The method returns a regularized DEM as a function of T. For the inversion, we have used zeroth-order regularization in the range of temperature log T (K) = 4.1 to log T (K) = 8.1 with 33 temperature bins having δlog T = 0.12 intervals [1]. Given the set of data from six AIA channels, we have obtained DEM for each pixel in the selected temperature range. The DEM maps at different temperatures show a similar spatial behaviour as in the SDO/AIA filters. Fig. 6.5 shows the DEM maps at different temperatures at logT (K) = 4.7, 5.6, 5.7, 5.8, 6.4, 6.7 at 05:18 UT. The DEM maps clearly indicate a multi-temperature

[1] http://www.astro.gla.ac.uk/~iain/demreg/

outflowing plasma. The base of the outflow region is giving higher emission values, indicating ongoing reconnection and heating processes.

6.3.4 Possible origin of impulsive plasma outflows

Using the HMI LOS magnetograms, we study the magnetic field evolution before and during the occurrence of impulsive outflow. The driving mechanism of the impulsive energy events can be inferred using SDO/HMI data.

Fig. 6.6 shows the sequence of HMI images taken on 30th March, 2011 showing the evolution of magnetic field aligned with the 1600 Å continuum image. The sequence of images having a box with bold lines overlaid on them shows the magnetic polarities at the footpoint of the brightening. The bigger dashed box represents the area taken around the negative polarity, and smaller dashed box represents the area around the positive polarity used to calculate the magnetic flux respectively. The arrow represents the flux cancellation site of two oppositely signed polarities where the negative polarity flux is found to be oscillating with time. In the last image, the contours of 1600 Å image are placed at the magnetic polarities associated with the brightening.

In the left panel of Fig. 6.7, the HMI contours are placed on the 1600 Å image where blue indicates the negative polatiy and red indicates the positive polarity. In the right panel of Fig. 6.7, the magnetic fluxes obtained from these polarities are plotted. The vertical dashed line represents the onset time of the outflow (i.e. 05:12 UT) and bold lines on the either side of the dashed line represent the duration for which wavelet analysis has been carried out (04:50:00 UT – 05:50:00 UT) on the derived negative magnetic flux. The magnetic flux emerging out of the negative polarity is increasing and further becomes almost constant when it cancels with the positive polarity in the vicinity. Also, the magnetic flux from the negative polarity shows an oscillatory behaviour during the flux cancellation and evolution of the outflow. The magnetic flux from these polarities is of the order of

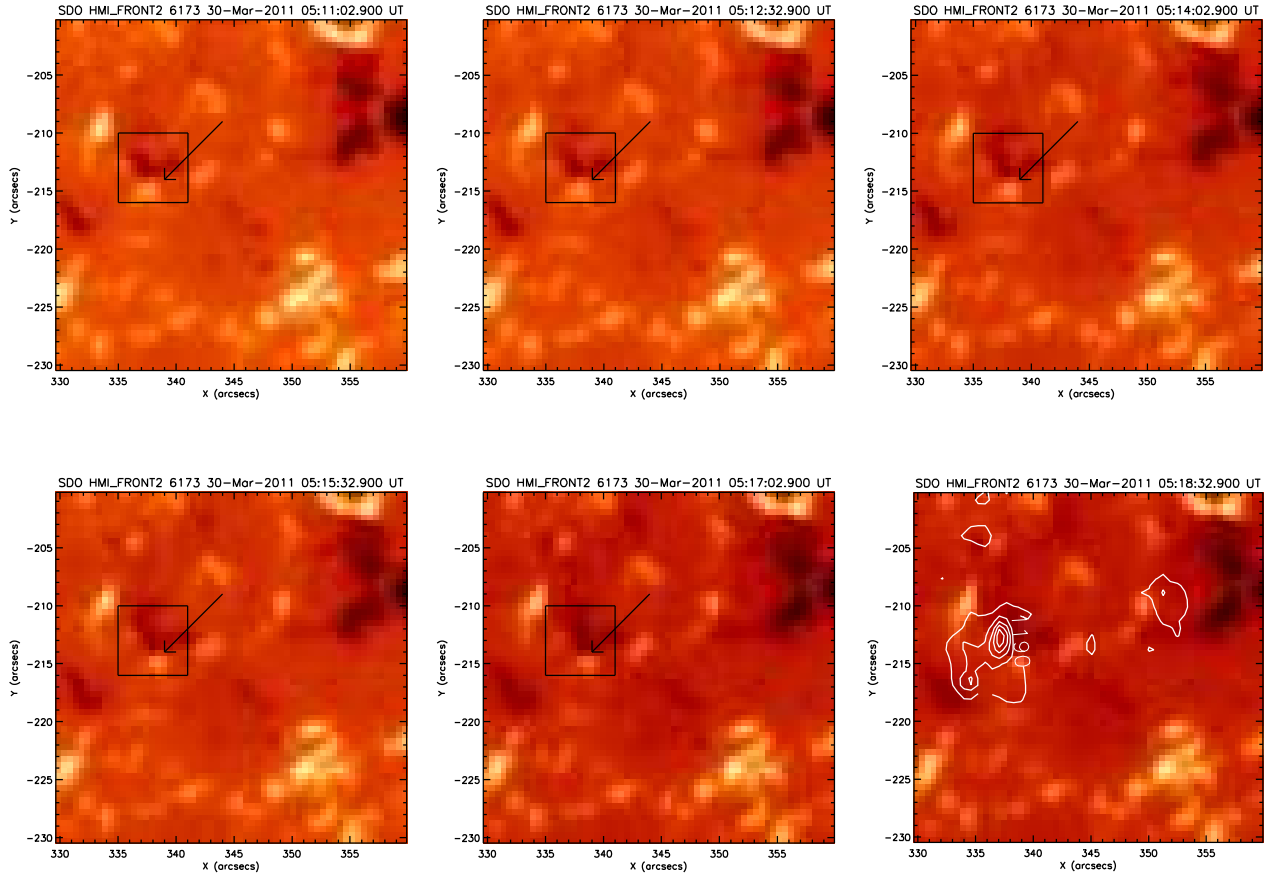

Figure 6.6: Time sequence of images taken from SDO/HMI showing the evolution of magnetic polarities from 05:11:02 UTC to 05:18:32 UTC at the footpoint of the outflow. The positive and negative polarities near the tip of the arrow corresponding to the energy releasing site leading to magnetic reconnection. The box with the bold lines encloses the magnetic polarities the footpoint of the brigtening. The bigger dashed box represents the area around the negative polarity and the smaller one represents the area around positive polarity which are used to calculate the magnetic flux. In the last image, the 1600Å continuum image contours are overlaid on the aligned HMI image.

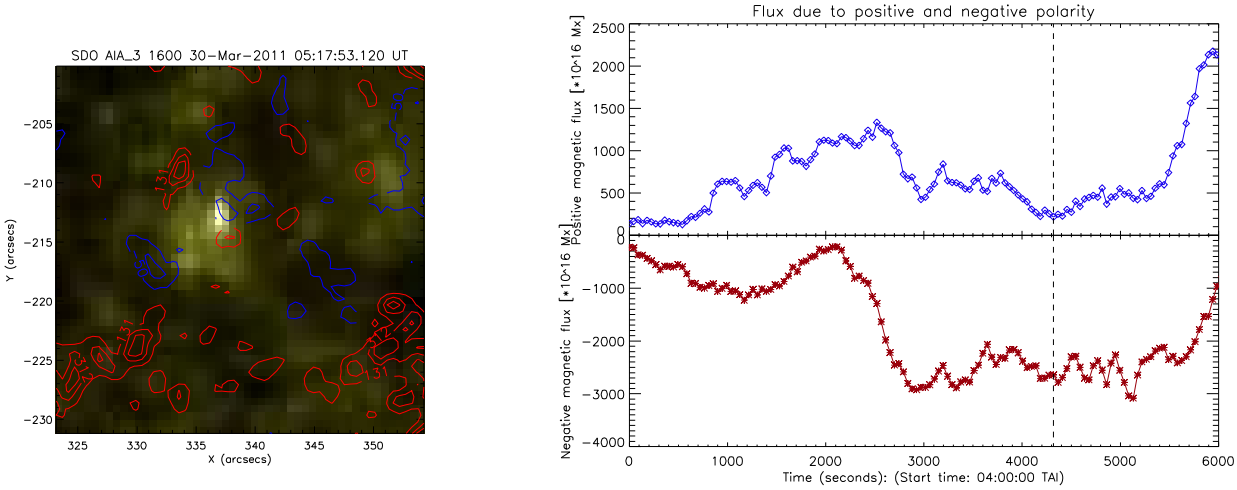

Figure 6.7: Left panel: HMI contours on the 1600 Å SDO/AIA image where blue indicates negative polarity and red indicates the positive polarity. Right panel: Plots showing the magnetic flux from the positive and negative polarities at the footpoint of the brightening. Vertical dashed line shows the onset time of the outflow and bold lines represent the duration for which wavelet analysis has been carried out.

10^{16} Mx. We derive the magnetic flux for 1 hr duration from the base of the outflow region (04:50:00 UT - 05:50:00 UT; Fig. 6.7). We also derive the 1600 Å flux from the base for the same duration (see Fig. 6.1).

Doyle & Phillips (1992) and Phillips et al. (1992) showed for both solar and stellar flares, the continuum at wavelength less than 1682 Å can be enhanced due to the ionization of neutral silicon atoms near the temperature minimum region irradiated by UV line radiation. Thus, the AIA 1600 Å filter can not be considered simply as entirely photospheric, but due to a contribution from the C IV double, the silicon continuum plus a contribution of the continuum by irradiation from C IV. Hence, some emission from this brightening as seen in the 1600 Å filter may arise from the higher solar atmosphere.

We carried out a wavelet analysis on the intensity curve of the 1600 Å image (04:50 UT – 05:50UT) and magnetic flux from the negative polarity of HMI (04:50 UT – 05:50UT). We use the standard procedure of wavelet analysis and randomization test to calculate

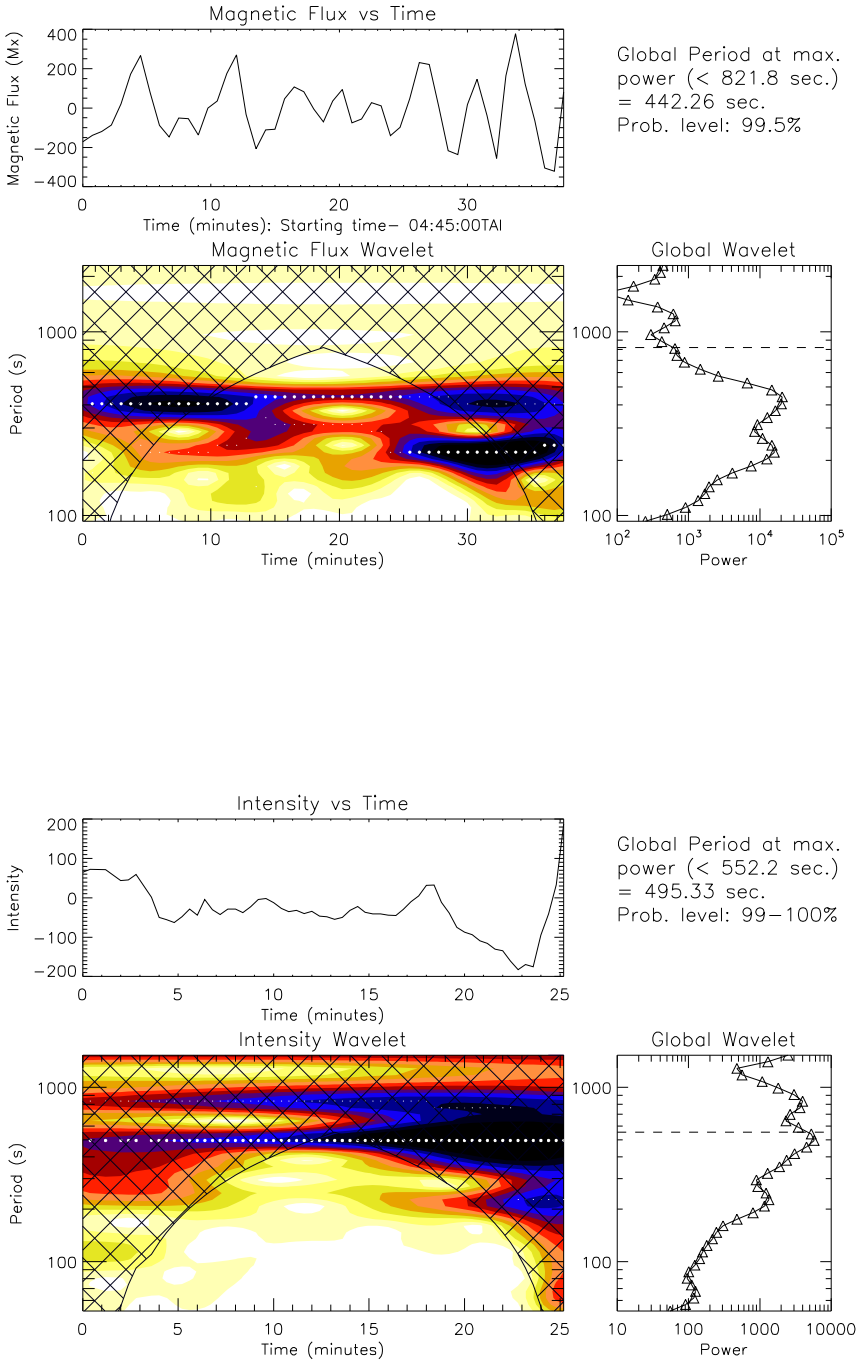

Figure 6.8: Top-panel: Wavelet analysis of the flux caused by the negative polarity. Bottom-panel: Wavelet analysis of the intensity curve obtained by 1600 Å SDO/AIA image.

the significance level of the periodicity (Linnell Nemec & Nemec, 1985; O'Shea et al., 2001). We notice the long term trends in the oscillatory behaviour of magnetic flux and 1600 Å flux, which are detrended and removed by box-car average by choosing the window-widths of '10' and '17', respectively. The fitted trend is shown in the bottom panel of Fig. 6.8. The background trend removal is a necessary step required to obtain the real oscillations present in the data, and the change of bin does not affect the wavelet results (e.g., Dwivedi & Srivastava, 2010; O'Shea et al., 2001). We determine the significant oscillation periods well below the COI and within the cone of influence (COI; O'Shea et al. (2001)). Fig. 6.8 shows the oscillation of about 442 s for the HMI magnetic flux and 416 s for 1600 Å with significance level of 99-100%. The wavelet results are found to be almost consistent with the power spectra estimated by periodogram (Scargle, 1982), which indicate the consistent presence of these real periodicities in the observed light curves (periodogram images are not shown). In both the panels (top and bottom) of Fig. 6.8, the evolution of magnetic flux and intensity as a function of time and oscillation periods are shown in the form of wavelet transforms which exhibit the dominant period of about P = $\approx$7.0 min. A slight difference in the detected periodicity lies well within the limit of uncertainity in estimating global power period.

The oscillations in magnetic flux and 1600 Å flux are present at the base of the outflows before, on the triggering time and even after the occurrence of the plasma outflow. This indicates the presence of magnetoacoustic waves mode at the base of the outflow region, which most likely create the oscillations in the small-scale current sheet enabling the reconnection and impulsive outflows (e.g., Heggland et al., 2009; McLaughlin et al., 2009, 2011, and references cited therein). The simultaneous oscillations in magnetic flux and intensity indicate the evolution of the magnetoacoustic waves in the magnetic domain at the base of the outflow. When magnetoacoustic waves see the discontinuity at the X−point (null point), these discontinuities develop into the fast oblique magnetic shock waves,

leading to the local heating of the plasma. These magnetoacoustic shocks above and below the X−point may form a triangular shock cusp (see observed cusp shape structure in the Fig. 6.1) that leads to the development of the hot plasma outflows (e.g., Heggland et al., 2009; McLaughlin et al., 2009, 2011). The magnetic reconnection may also be associated with this region in the form of the change of magnetic connectivity (McLaughlin et al., 2009), which is evident as the morphological changes occurring at the base of the outflow. The continuous positive and negative flux cancellation is also evident at the footpoints of the brightening that may also contribute to the associated outflows (Figs. 6.6 and 6.7).

6.4 Discussion and Conclusions

In this chapter, we have used multi-wavelength observations and muti-instrument datasets for our study. We have presented a small-scale impulsive plasma outflow from the photosphere/lower chromosphere to the outer layers of the Sun that is co-temporal with an increased emission from the SDO/AIA transition region and coronal filters. The main points of this impulsive small-scale plasma outflow are as follows:

1. The transient is a small scale energy release site of ≈8" lasting for ≈8 min and driving energy to the upper atmosphere.

2. The top of the small-scale energy release site consists of a plasma outflow which rises 30 Mm in a very short span of the time with an apparent velocity of the outflow of 1250 km s^{-1}.

3. It is generated in a small-scale current sheet and driven by magnetoacoustic waves/shocks.

4. A DEM analysis indicates a multi-temperature plasma over the temperatures ranging from the lower chromosphere to the coronal region.

5. The topological behaviour of the magnetic polarities at the footpoint of the brightening indicated cancellation.

6.Oscillations in 1600 Å flux and the negative magnetic flux indicate that the magnetoa-

coustic waves are present at the base of the outflow region in the small-scale current sheet, which further lead to the outflows (Fig. 6.1).

The continuous positive and negative flux cancellation is also evident at the footpoints of the brightening. In conclusion, the wave- driven energy release at the X-point and overlying cusp (Fig. 6.1) and flux cancellation at the footpoint collectively in the lower magnetic domain (or configuration) of the plasma outflow region trigger this gigantic motion.

The unique feature of the impulsive plasma outflow considered for our study is having high apparent velocity of 1250 km s^{-1}, transporting mass and energy from the lower atmosphere to the upper atmosphere. Understanding the driving mechanism of such impulsive plasma outflows is a first step in understanding its role in plasma dynamics. Such outflows in abundant measure may act as a significant sources for energy and mass transport in the lower solar corona.

Shibata (1982) suggested the classification of the jets into two types on the basis of the height of the energy release site. If the height of the energy release reconnection site is lower than the critical height of the jet/outflow then it will be driven by crest shocks and directly by pressure gradient force due to an explosion if it is greater. Similar studies regarding surges has been conducted by (Kayshap et al., 2013). Surges differ from the thermal pulse driven jets since magnetic forces also come into play for their acceleration. Therefore, pervasive magnetoacoustic shocks may be a plausible trigger mechanism in the lower part of the solar atmosphere during X-point reconnection in generating jets (Heggland et al., 2009). Although in the present case, the physical conditions are somewhat different. As stated above, the impulsive outflow taken for our study shows the signatures of flux cancellation at the photosphere as well as small-scale current sheet, leading to the evolution of the magnetoacoustic wave driven shocks at the X−point at the inner coronal height (e.g., 5 Mm from footpoint; Fig. 6.1).

This further also enables the magnetic reconnection at the coronal heights (McLaughlin et al., 2009). The presence of the magnetoacoustic waves around the X−point pushes this point of discontinuity and creates the magnetoacoustic shocks, related shock cusp and associated outflows (Fig. 6.1). This is also associated with the reconnection of magnetic field lines and energy generation at the coronal height near the cusp, which may drive the outflow with nearly Alfvén speed (here speed is 1250 km s^{-1}) by direct $\vec{j} \times \vec{B}$ forces (Cirtain et al., 2007; McLaughlin et al., 2011; Nishizuka et al., 2008).

These observations provide us with an evidence of highly impulsive plasma outflows caused by the magnetoacoustic waves and evolved shock at the small-scale cusp (and X−point) associated with a small-scale current sheet, which we have detected due to high spatial and temporal resolution of AIA vis-á-vis HMI data.